Computational Organometallic Chemistry with Force Fields

Jing Huang, Michael Devereux, Franziska Hofmann, and Markus Meuwly

Abstract This chapter discusses molecular mechanics (MM)-based approaches to investigate organometallic complexes. In particular, ligand field MM (LFMM), "Sum of Interactions Between Fragments *Ab Initio*" (SIBFA), and VALBOND with its extension to VALBOND-TRANS are presented in some detail. Two particular applications of VALBOND-TRANS to an Ir(III) and a Pt(II) complex are presented. Possible future extensions, including the study of chemical reactions and polarization effects, are briefly discussed at the end.

1 Introduction

Theoretical and computational methods can be very helpful for understanding and predicting structure and reactivity in organometallic chemistry. Over the past decade, quantum chemical methods—in particular density functional theory (DFT)—have made steady progress in addressing questions of practical relevance for increasingly complex systems. Especially hybrid functionals including B3LYP [1, 2] have been found to provide good accuracy for a range of properties at moderate computational cost. However, despite the continuing effort in devising

J. Huang • F. Hofmann
Department of Chemistry, University of Basel, Klingelbergstr 80, Basel CH 4056, Switzerland

M. Devereux
Department of Chemistry, University of Basel, Klingelbergstr 80, Basel CH 4056, Switzerland

IFR Laboratoire de Chimie et Biochimie Pharmacologique et Toxique, Université Paris Descartes, Paris, France

M. Meuwly (✉)
Department of Chemistry, University of Basel, Klingelbergstr 80, Basel CH 4056, Switzerland

Department of Chemistry, Brown University, Providence, RI, USA
e-mail: m.meuwly@unibas.ch

O. Wiest and Y. Wu (eds.), *Computational Organometallic Chemistry*,
DOI 10.1007/978-3-642-25258-7_2,

more general and more accurate functionals, all quantum methods invariably reach a point where they become computationally too demanding. In most cases, DFT calculations are limited to geometry optimizations of gas-phase structures or to model systems with smaller and sometimes unrealistic ligands. Dynamics simulations and calculations over large libraries of compounds are often impractical, and including the effect of solvent beyond implicit models is typically impossible. Therefore, having faster, even if approximate methods is desirable. Molecular mechanics (MM) force fields such as AMBER [3], CHARMM [4], or OPLS [5] have become standard methods in biomolecular chemistry and are routinely used for molecular dynamics simulations of systems with up to one million atoms. However, the development of general force fields for transition metal complexes has been relatively limited because of the unique difficulties presented by these types of compounds [6–8]: metals can have a variety of coordination numbers, π-binding ligands can bind in various ways, and electronic effects such as Jahn–Teller distortion or the trans influence need to be addressed.

The realization that the electronic Schrödinger equation can only be solved for small systems led to the development of important alternative approaches to study chemical reactivity. They date back to London's work on the $H+H_2$ reaction for which he used a 2×2 valence bond treatment [9]. Building on this, refined and extended approaches led to the London–Eyring–Polanyi (LEP) [10] and the London–Eyring–Polanyi–Sato (LEPS) surfaces [11, 12]. A development that continued the efforts to use valence bond theory to describe multistate chemical systems is the diatomics-in-molecules (DIM) theory [13]. Following a slightly different perspective, Pauling profoundly influenced the theoretical description of chemical reactivity through his work on molecular structure and the nature of the chemical bond [14, 15]. Significant relations, such as the one between bond length and bond order, later became foundations to empirical descriptions of reactivity [16, 17].

Explicit exclusion of all electronic effects leads to empirical force fields (FF). They were developed with the emphasis to carry out studies of the structure and dynamics of macromolecules, including peptides and proteins [3, 5, 18–23]. Thus, their primary application area was sampling and characterizing conformations of extensive molecular structures. The mathematical form of a generic FF is $V_{\text{tot}} = V_{\text{bond}} + V_{\text{valence}} + V_{\text{dihe}} + V_{\text{elstat}} + V_{\text{vdW}}$, where each of the terms is separately parametrized

$$
\begin{aligned}
V_{\text{bond}} &= \sum K_{\text{b}}(r - r_{\text{e}})^2, \\
V_{\text{valence}} &= \sum K_{\theta}(\theta - \theta_{\text{e}})^2, \\
V_{\text{dihe}} &= \sum K_{\phi}(1 + \cos(n\phi - \delta)), \\
V_{\text{elstat}} &= \frac{1}{4\pi\varepsilon_0} \sum \frac{q_i q_j}{r_{ij}}, \\
V_{\text{vdw}} &= \sum \varepsilon_{ij} \left[\left(\frac{R_{\text{min},ij}}{r_{ij}} \right)^{12} - \left(\frac{R_{\text{min},ij}}{r_{ij}} \right)^{6} \right].
\end{aligned}
\tag{1}
$$

The first three terms comprise "bonded" interactions, while the latter two describe the "nonbonded" ones. In these expressions, K represents the force constants associated with the particular type of interaction, r_e and θ_e are equilibrium values, n is the periodicity of the dihedral, and δ is the phase which determines the location of the maximum. The sums for the bonded terms are carried out over all atoms involved. Nonbonded interactions include electrostatic and van der Waals terms where the sums include all nonbonded atom pairs. q_i and q_j are the partial charges of the atoms i and j involved and ε_0 is the vacuum dielectric constant. For the van der Waals terms, the potential energy is expressed as a Lennard-Jones potential with well depth $\varepsilon_{ij} = \sqrt{\varepsilon_i \varepsilon_j}$ and range $R_{\min,ij} = (R_{\min,i} + R_{\min,j})/2$ at the Lennard-Jones minimum. This interaction captures long-range dispersion ($\propto -r^{-6}$) and exchange repulsion ($\propto r^{-12}$) where the power of the latter is chosen for convenience. The set of expressions in (1) constitutes a minimal model for a force field which might be extended by using explicit terms for hydrogen bonds or for metal-containing systems [24].

Building on the success of FFs for "simple" chemical and biological systems, attempts were made to not only retain their functional simplicity but also encode additional functionality to treat metal-containing systems. In the following, we describe several attempts to do this and discuss particular applications relevant to our own work. The chapter ends with an outlook.

2 Conceptual Approaches

In the following section, different techniques to investigate the energetics and dynamics of organometallic systems based on extensions of force field concepts are discussed.

2.1 Ligand Field Molecular Mechanics

Ligand field theory (LFT) can be considered as a combination of crystal field theory (CFT) and molecular orbital (MO) theory [25]. Unlike in CFT where interactions between ligands and center metal atoms are described with electronic interactions, LFT takes into account the overlap between atomic orbitals as ligands approach a metal center. Thus in LFT, the metal–ligand bonding is by its very nature partially covalent.

LFT is very successful in explaining magnetic and spectral properties of many transition metal complexes. In its framework, the perturbation Hamiltonian for separate ligands interacting with the metal center is assumed to be independent and additive. Thus, LFT can in principle be introduced into a MM force field. The first successful combination was made by Burton et al. [26]. Afterwards, Deeth and coworkers [24, 27–32] developed the approach gradually into a force field called

Ligand Field Molecular Mechanics (LFMM). Thus, LFMM is based on a combination of a conventional force field with terms explicitly capturing electronic effects, which takes the following functional form:

$$E_{\text{tot}} = E_{\text{bonds}} + E_{\text{angles}} + E_{\text{dihedrals}} + E_{\text{nonbonded}} + \text{LFSE}. \tag{2}$$

The essential part in (2) is the ligand field stabilization energy (LFSE). In LFMM, such an energy is obtained by diagonalizing a 5 × 5 ligand field potential matrix, with elements

$$\langle d_i | V_{\text{LF}} | d_j \rangle = \sum_{l}^{N} \sum_{k}^{3} F_{i,k}^{l} F_{k,j}^{l} e_k^l. \tag{3}$$

The first summation (l) is over all N metal–ligand interactions, while the second summation runs over three symmetry modes ($k = \sigma, \pi_x, \pi_y$). Whether certain symmetry modes are included or not depends on the ligand type. For example, only one term e_σ is required for saturated amines because they cannot interact with the metal through π-bonding [26].

In (3), the radial and angular parts of the M–L interactions are separated. The general form of a radial contribution e_λ is given by

$$e_\lambda = a_0 + a_1 r + a_2 r^{-2} + a_3 r^{-3} + a_4 r^{-4} + a_5 r^{-5} + a_6 r^{-6}, \tag{4}$$

where r is the metal–ligand bond length. In practice, most coefficients a_i zero and only one or two terms in (4) take effect, which decreases the number of force field parameters that need to be fitted.

All the angular dependence is encoded in the F factors as defined in the angular overlap model (AOM) [33, 34]. These angular overlap factors characterize the angular dependence of overlap integrals between atomic orbitals of the center atom and the ligand atom. A detailed expression of F functions in the ligand's angular coordinates (θ, φ, ψ) has been worked out by Schaeffer [35] and can be found in Table 1 in [34]. For instance, considering an octahedral complex with O_h symmetry, the six ligands have the following angular coordinates with respect to the metal center:

	1	2	3	4	5	6
θ	0	$\frac{\pi}{2}$	$\frac{\pi}{2}$	$\frac{\pi}{2}$	$\frac{\pi}{2}$	π
ϕ	0	0	$\frac{\pi}{2}$	π	$\frac{3\pi}{2}$	0

and if the ligand is unidentate, ψ may take an arbitrary value, e.g., 0. Then for the first ligand,

$$\begin{aligned} F^1_{z^2,\sigma} &= (1 + 3\cos 2\theta)/4 = 1, \\ F^1_{yz,\pi^y} &= \cos\phi\cos\theta\cos\psi - \cos\phi\cos 2\theta\sin\psi = 1, \\ F^1_{zx,\pi^x} &= -\sin\phi\cos\theta\sin\psi + \cos\phi\cos 2\theta\cos\psi = 1, \end{aligned} \tag{5}$$

and all the other F values equal zero. Similarly, all the non-zero F values for the fifth ligand are

$$\begin{aligned} F^5_{z^2,\sigma} &= (1 + 3\cos 2\theta)/4 = -\frac{1}{2}, \\ F^5_{x^3-y^2,\sigma} &= \frac{\sqrt{3}}{4}\cos 2\phi(1 - \cos 2\theta) = -\frac{\sqrt{3}}{2}, \\ F^5_{xy,\pi^y} &= \cos 2\phi \sin\theta \cos\psi - \frac{1}{2}\sin 2\phi \sin 2\theta \sin\psi = -1, \\ F^5_{yz,\pi^x} &= \cos\phi \cos\theta \sin\psi + \sin\phi \cos 2\theta \cos\psi = 1. \end{aligned} \tag{6}$$

Two additional energy terms e_{ds} and e_{pair} are then introduced to the LFSE for completeness, and they also take the functional form (4). The d–s mixing term, e_{ds}, characterizes the mixing between valence s orbital and d orbitals of the metal atom with matching symmetry. For example, in a planar D_{4h} $[CuCl_4]^{2-}$ system, such a configuration interaction between Cu 4s orbital with $3d_{z^2}$ need to be included to obtain the correct relative energies. The interelectronic repulsion term, e_{pair}, captures the effect of the two-electron d–d electrostatic interactions and is important for predicting the actual spin state.

The total LFMM energy is, therefore, calculated from an electronic term (LFSE) and additional terms that can be obtained from a conventional force field, such as AMBER [3], CHARMM [4], or the more complex MMFF [36]. Caution is needed when handling the energy terms involving metal atoms, such as the explicit metal–ligand bond energy $E_{\mathrm{M-L}}$. The functional forms may need to be adjusted and parameters refitted to lead to correct coordination geometries. For example, $E_{\mathrm{M-L}}$ is better described by a Morse function

$$E_{\mathrm{M-L}} = D_{\mathrm{e}}\{1 - \exp[\beta(r - r_0)]\}^2 - D_{\mathrm{e}} \tag{7}$$

with three parameters D_{e}, β, and r_0. Besides, the explicit L1–M–L2 angle bend term should be replaced by a simple ligand–ligand repulsive term to avoid double counting of energy.

The complete LFMM force field has been implemented in the molecular operating environment (MOE) as an extension named DommiMOE (d orbital molecular mechanics in MOE) [28]. LFMM has been applied extensively to copper complexes, from simple Cu(II) amines [29] to copper enzymes [32], and a variety of force field parameters for copper complexes are available. The parametrization is done by fitting the parameters in (4) to the crystallographic structure data provided by the Cambridge Structural Database [29, 30], while DFT calculation results are sometimes also involved in the fitting [32].

LFMM parameters for other transition metal complexes, such as manganese-, nickel-, and zinc-containing complexes, are also provided by Deeth and coworkers following a similar parametrization protocol [26, 30, 31]. The majority of applications of LFMM force fields concerns "first-low" transition metal complexes,

since the LFT is based on the assumption that the d shell of the metal center is weakly affected by the ligand environment. Applications to organometallic compounds are possible [27], but a valence bond approach based on hybridization schemes might be more feasible.

2.2 SIBFA

An alternative approach to modeling organometallic complexes within a classical molecular mechanics framework is the "Sum of Interactions Between Fragments Ab Initio" (SIBFA) method. Development of this force field began in the 1980s, with contributions from Claverie, Gresh, and Piquemal, among others [37–40]. SIBFA is a fragment-based approach employing a detailed force field that has been widely applied to organometallic systems, from small complexes to metalloproteins [41–44]. The force field explicitly accounts for anisotropic fragment polarization, repulsion and charge transfer, and incorporates distributed multipole moments centered at both nuclear positions and bond barycenters to describe electrostatics. The additional detail afforded by these energetic terms makes SIBFA more computationally expensive than less detailed force fields such as CHARMM [4] and AMBER [3], but as a consequence, SIBFA can yield molecular structures and energies that are in close agreement with ab initio data while maintaining a much lower computational overhead than would be required for a full ab initio computation. While the standard, most widely applied version of SIBFA affords close agreement in calculated interaction energies with ab initio reference data for a wide range of organic compounds and closed-shell organometallic systems (metals including Mg(II), Ca(II), Zn(II), and Cd(II)), a recent extension "SIBFA-LF" including ligand field effects via the AOM has extended the range of application to metal ions such as Cu(II) with partially filled d-shells. Both SIBFA and SIBFA-LF will be described in more detail in the following sections with examples of successful application of the method.

The basic premise of SIBFA is to build a force field that can account for each of the terms of an energy decomposition of the ab initio intermolecular interaction energy, as defined within the Restricted Variational Space Approximation (RVS) of Stevens and Fink [45]. Within the RVS scheme, the total interaction energy is broken down into first-order Coulomb (E_c) and exchange-repulsion (E_e) energies, and second-order polarization (E_{pol}) and charge transfer (E_{ct}). Agreement with correlated post-Hartree–Fock methodologies is achieved by inclusion of an additional dispersion energy term [46]. Faithful reproduction of these terms within the force field, including ligand dependence, radial dependence, and anisotropy, allows SIBFA to account for the total ab initio interaction energy for any conformation of an arbitrary complex as long as general parameters for the metal center and the fragments required to build up the ligands exist. In addition, short-range energetic corrections allow SIBFA to describe the formation of ligand–metal complexes without resorting to separate bonded and nonbonded parameters to describe the

bound and unbound states. A single, consistent parameter set is used to explore the binding, dissociation, and the relative energies of different tautomers and conformers. One limitation of the SIBFA approach is that parameters are only fitted for minimum energy conformers of each fragment used to build a molecule or complex. Individual fragment geometries are therefore kept frozen. This allows only torsional degrees of freedom within a molecule about fragment connection points, a limitation that is currently being addressed along with implementation of analytical gradients to allow the future application of SIBFA to molecular dynamics simulations.

Electrostatic Interaction Energy: Multipole moments used in SIBFA are derived from the ab initio charge density according to the procedure of Vigne-Maeder and Claverie [47]. E_{mtp} is truncated at quadrupole–quadrupole interactions. The sharing of multipoles between both atom and bond centers ensures improved short-range convergence of E_{mtp}. A recently extended formulation [42] also includes a penetration contribution to account for the overlap of molecular charge densities. Penetration becomes important at short range where significant overlap of the electron density of separate atoms or molecules takes place, and a standard multipolar expansion breaks down. Explicitly accounting for overlap is, therefore, necessary to achieve good agreement in the Coulomb energy with RVS results, and thereby with the total ab initio interaction energy. The multipolar interaction energy E_{mtp} between all atoms in fragment $\mathcal{A}$ and those in $\mathcal{B}$ without penetration is expressed using spherical tensor formalism as [48, 49]

$$E_{\mathrm{mtp}}(\mathcal{A},\mathcal{B}) = \frac{1}{2}\sum_{A\in\mathcal{A}}\sum_{B\in\mathcal{B}} E_{\mathrm{mtp}}(\mathbf{A},\mathbf{B}), \tag{8}$$

$$E_{\mathrm{mtp}}(\mathbf{A},\mathbf{B}) = \sum_{l_A l_B k_A k_B} T_{l_A l_B k_A k_B}(\mathbf{r}_{AB})\, Q_{l_A k_A} Q_{l_B k_B}. \tag{9}$$

The sum in (8) runs over all multipolar centers (nuclei and bond barycenters) of fragments $\mathcal{A}$ and $\mathcal{B}$. The interaction energy E_{mtp} between the multipoles on two sites with position vectors $\mathbf{A}$ and $\mathbf{B}$ is calculated by summing the product of a geometrical tensor T and each multipole moment Q. Multipole moments are expressed using spherical harmonics with rank l, k, where $l = 0, 1, 2$. T is used to relate the local axis systems of the multipolar sites A and B separated by vector $\mathbf{r}_{AB}$.

The modified electrostatic interaction energy, including penetration, includes an additional energetic dependence of the monopole–monopole and monopole–dipole terms on the number of valence electrons present in each overlapping site. Only the monopole–monopole and monopole–dipole terms are currently corrected as they dominate the total electrostatic energy in most situations. The monopole–monopole term for atoms A and B with monopoles q_A and q_B and number of valence electrons Z_A and Z_B separated by distance r is then defined as

$$E_{\text{mono-mono}} = [Z_A Z_B - \{Z_A(Z_B - q_B)(1 - \exp(-a_B r_{AB})) - Z_B(Z_A - q_A)(1 - \exp(-a_A r_{AB}))\} + (Z_A - q_A)(Z_B - q_B)(1 - \exp(-b_A r_{AB}))\,(1 - \exp(-b_B r_{AB}))](1/r_{AB}). \quad (10)$$

For monopoles centered on bonds, Z is equal to zero. In the limit of large separation r_{AB}, this expression converges toward the familiar Coulomb charge–charge interaction energy. The parameters a_A and b_A are obtained from $a_A = \gamma/R_{\text{w}A}$ and $b_A = \delta/R_{\text{w}A}$, where γ and δ are two unitless constants that have been calibrated as 4.42 and 4.12, respectively [40]. $R_{\text{w}A}$ is the van der Waals radius of the atom, or where bond multipoles are concerned, the averaged radius over the two atoms involved in the bond. The modified charge–dipole term is then obtained from the scalar product

$$E_{\text{mono-dip}} = -\mu_B \times \xi_A^*(\mathbf{B}). \quad (11)$$

μ is the dipole moment of site B. In the uncorrected multipolar interaction energy, $\xi_A^*(\mathbf{B})$ represents the electric field created by monopole A at point B with position vector $\mathbf{B}$, $\xi_A(\mathbf{B}) = q_A \mathbf{r}_{AB}/r_{AB}^3$, where $\mathbf{r}_{AB}$ is the vector running from site A to site B. The corrected monopole–dipole term including an overlap contribution is

$$\xi_A^*(\mathbf{B}) = \{Z_A - (Z_A - q_A)(1 - \exp(-\eta r_{AB}))\}\mathbf{r}_{AB}/r_{AB}^3 \quad (12)$$

$$\eta = \chi/((R_{\text{w}A} + R_{\text{w}B})/2), \quad (13)$$

where χ is a unitless constant equal to 2.4. While this penetration correction clearly adds complexity to the evaluation of an electrostatic interaction, the complexity is easily justifiable in the case of metal complexes where metal and ligand atoms approach particularly close to one another, and charged metal ion centers produce a strong short-range electrostatic interaction energy. The ability to evaluate short-range interactions then avoids the need for separate "bonded" and "nonbonded" terms between the metal ion and complexed ligands.

Short-Range Repulsion: Strong short-range Pauli repulsion between same-spin electrons is modeled in SIBFA using a sum of bond–bond, bond–lone pair, and lone pair–lone pair interactions. Bond sites are again located at the barycenters between bonded atoms inside a fragment. Simpler, isotropic repulsion terms do not account for orientational dependence of the repulsion energy. The relative orientation of bound complexes is, therefore, determined not only by the anisotropic electrostatic interaction, but at close range also by anisotropic electron pair repulsion. While valence electron pairs are involved in bond formation and are hence found between bonded atoms, additional nonbonded valence lone pairs must also be taken into account for atom types such as oxygen and nitrogen. The positions of these electron lone pairs must be defined, and one means of achieving this is the electron localization function (ELF) originally proposed by Becke and Edgecombe [50]. Once the centroids of localized orbitals have been located using ELF in ab initio calculations, then their coordinates can be stored in SIBFA in the fragment's local axis system.

The distance between two interacting centroids r_{ij} on separate fragments can then be used to approximate the degree of overlap of the electron pairs S, and hence used to estimate the repulsion energy in SIBFA according to [42]

$$\mathrm{rep}(i,j) = N_{\mathrm{occ}}(i)N_{\mathrm{occ}}(j)\left[c_1 S^2(i,j)\Big/ r_{ij} + c_2 S^2(i,j)\Big/ r_{ij}^2\right]. \tag{14}$$

$N_{\mathrm{occ}}(i)$ is the occupation number of orbital i (equal to 2 for doubly occupied bonds and lone pairs, 1 for π-type lone pairs), c_1 and c_2 are multiplicative constants that are to be fitted for an atom type using the ab initio energies of a series of reference complexes in different geometries. Note that the r_{ij}^2 correction has recently been added in accord with the original proposal of Murrell and Teixeras-Dias [51]. The total repulsion between atoms is evaluated between all lone pair and bond combinations so that the repulsion between atom A involved in bonds b_A with lone pairs L_A and atom B involved in bonds b_B with lone pairs L_B is the sum of all pair–pair interactions [52]

$$\begin{aligned} E_{\mathrm{rep}} = c_1 \Bigg(& \sum_{b_A}\sum_{b_B} rep\,(b_A, b_B) + \sum_{b_A}\sum_{L_B} rep\,(b_A, L_B) \\ & + \sum_{L_A}\sum_{b_B} rep\,(L_A, b_B) + \sum_{L_A}\sum_{L_B} rep\,(L_A, L_B) \Bigg). \end{aligned} \tag{15}$$

The remaining orbital overlap term S is approximated using tabulated orbital coefficients and effective atomic radii for the atom in the fragment of interest. Further details are to be found in [52].

Charge Transfer: Charge transfer becomes important where metal–ligand bonds exhibit some degree of covalent character. Electron density from the bound ligands can be transferred to the central metal cation M, and back donation to or from the d-orbitals of transition metals can provide an additional energetic contribution. Charge transfer in SIBFA is based on the expression [53–55]

$$E_{\mathrm{ct}} = -2c_{\mathrm{M}} \sum_{a \in L_A} N_{\mathrm{occ},a}\left((I_{a,\mathrm{M}^*})^2 \Big/ \Delta E_{a,\mathrm{M}^*} \right). \tag{16}$$

The summation runs over all electron pairs L belonging to the electron donor-atom A of fragment $\mathcal{A}$. The constant c is characteristic of the metal cation M, the occupation number of the electron pair N_{occ} is multiplied by an integral I describing overlap of the donor lone pair and acceptor cation, and by $\Delta E_{a,\mathrm{M}*}$, the difference between the lone pair ionization potential and the acceptor atom electron affinity. This integral has been approximated within a classical molecular mechanics framework using the distance and angles between orbital centroids containing electron lone pairs. The positions of these orbital centroids in the fragment's local axis system are identified in the same way as for the repulsion term E_{rep}. The form of the

expression and the derivation from the full overlap integral are given in detail in [39, 53, 56, 57]. In addition, as the charge transfer energy in certain divalent cation complexes represents a significant contribution to the total interaction energy, a series of corrections have been made to increase its accuracy. In these corrections, metal and ligand properties such as atomic radius and electron affinity are allowed to alter as a function of the electric field that they encounter. Full details of these modifications are found in [39].

Polarization: Electron polarization makes the final major contribution to the total interaction energy in the standard SIBFA force field. A second-order correction to the electrostatic interaction energy, polarization affects primarily the outer valence electrons of an atom. As such, polarizable sites in SIBFA are located at the same bond barycenter and electron lone pair sites used to calculate the Pauli repulsion energy E_{rep}. The polarization energy takes the form of an interaction between an induced dipole and the electric field generated by surrounding moieties, and an induced quadrupole with the field gradient (induced quadrupoles are applied to metal cations only). The magnitude of the induced dipole is [42]

$$\mu_{i,p}^{\text{ind}} = \alpha_{ij,p}\, \xi_j(\mathbf{p}). \tag{17}$$

$\alpha_{ij,p}$ represents an element i, j of the 3×3 polarizability tensor of polarizable site p acting on component i (x, y or z) of the induced dipole moment $\mu_{i,p}^{\text{ind}}$ as a result of component j of the electric field ξ at $\mathbf{p}$. The total electric field at $\mathbf{p}$, the position vector of site p belonging to fragment $\mathcal{A}$, is obtained using

$$\xi_j(\mathbf{p}) = \sum_{\mathcal{B}\neq\mathcal{A}} \sum_{m\in\mathcal{B}} \xi_{j,m}(\mathbf{p}). \tag{18}$$

The first sum is over each fragment $\mathcal{B}$ interacting with $\mathcal{A}$, and the second sum is over all multipolar sites m of fragment $\mathcal{B}$ that give rise to an electric field. Note that sites within the same fragment do not interact, and certain terms are removed from the interaction between atoms at the connection points of two fragments that are covalently bonded in a larger molecule. Central metal atoms and coordinated ligands are, however, not treated as covalently bonded fragments and are allowed to interact fully. Partial covalent character is then encapsulated by charge transfer and short-range contributions such as penetration. A screening term intervenes in the polarization energy at very close range to prevent close contact between charge-carrying sites of one moiety and polarizable sites of another, giving rise to non-physical polarization energies. A Gaussian function g screens the electric field ξ arising from multipolar site m at polarizable site p according to

$$\xi_m(\mathbf{p}) = (1 - g(r_{pm}))\xi_m^0(\mathbf{p}), \tag{19}$$

$$g(r_{pm}) = q_m K_1 \exp[-K_2(r_{pm}^2/(R_{1\text{w}p} + R_{1\text{w}m}))], \tag{20}$$

where r_{pm} is the distance between polarizable site p and multipolar site m with monopole moment q_m, R_{1wp} is the effective radius of the atom containing site p, and R_{1wm} is the effective radius of the atom containing multipolar site m. For sites located on a barycenter, the effective radius used is the average of the two atoms that make up the bond. K_1 and K_2 are parameters fitted for the moiety of interest [39]. The total polarization energy of p is then

$$E_{\mathrm{pol},p} = -0.5 \sum_i \xi_i^0(\mathbf{p}) \sum_j \alpha_{ij,p}\, \xi_j(\mathbf{p}) \tag{21}$$

with $\xi_i^0(\mathbf{p})$ as component i of the electric field at $\mathbf{p}$ due to the permanent multipoles of all interacting sites. $\xi_j(\mathbf{p})$ is component j of the electric field due to the sum of the permanent and induced multipoles. As the electric field involves the induced multipoles of surrounding moieties, an iterative, self-consistent procedure is used. The quadrupolar polarizability is implemented in a similar fashion, describing the second-order correction to the quadrupole moment of each site m arising from interaction with the electric field gradient [42].

Ligand Field Effects: In order to extend the range of application of the SIBFA force field to metals with partially filled d-shells such as Cu(II) with clear biological importance, a LFSE based on the same AOM introduced in the LFMM approach was recently added [38]. The total interaction energy of a metal–ligand complex (including a dispersion term E_{disp} for improved agreement with correlated ab initio methods) [46] in SIBFA-LF is defined, therefore, as

$$E_{\mathrm{int}} = E_{\mathrm{mtp}} + E_{\mathrm{rep}} + E_{\mathrm{pol}} + E_{\mathrm{ct}} + E_{\mathrm{disp}} + E_{\mathrm{LFSE}}. \tag{22}$$

The first four terms are the Coulomb, repulsion, polarization, and charge transfer energies, respectively. As previously described, the LFSE E_{LFSE} arises from the interaction of metal d-orbitals with surrounding ligands. The degree of overlap of a d-orbital with a given ligand again depends on the distance and relative orientation, as can be ascertained from an overlap integral. The AOM overlap integral for SIBFA is also divided into angular and radial contributions. The radial component of the overlap is approximated using an exponential decay [58] $e_\lambda = a + b \exp(-cr_{\mathrm{ML}})$, where a, b, and c are parameters specific to the metal–ligand pair and r_{ML} is the metal–ligand separation. The angular component of the overlap is then described using second-order ($l = 2$) spherical harmonics to describe d-orbital shapes. The spherical harmonics give rise to angular coefficients D that describe the degree of overlap between a ligand σ-orbital and a metal d-orbital i as a function of the polar coordinates θ and φ between them [38] (Table 1).

The coefficients are combined with the radial term e_λ to construct a simplified Hamiltonian describing the d-orbital energies. Note that e_λ represents a radial correction due to LFSE only, and that the primary contribution to the radial dependence of the ligand–metal interaction energy comes from the standard

Table 1 Angular coefficients between metal d-orbitals and ligand σ bonding orbitals

i	$D_i(\theta, \phi)$
z^2	$1/2(3\cos^2\theta - 1)$
yz	$1/2(\sqrt{3}\sin 2\theta \sin\phi)$
xz	$1/2(\sqrt{3}\sin 2\theta \sin\phi)$
xy	$1/4(\sqrt{3}(1-\cos 2\theta)\sin 2\phi)$
$x^2 - y^2$	$1/4(\sqrt{3}(1-\cos 2\theta)\cos 2\phi)$

energetic terms listed in (22). Each element of the Hamiltonian matrix represents a sum of the overlap with every ligand l

$$\mathcal{H}_{dd'} = \sum_l e_\lambda^l \langle d|l\rangle\langle l|d'\rangle. \tag{23}$$

The final relative energy ε of each of the i d-orbitals is then obtained from the Hamiltonian matrix by diagonalization. Note that only bonds to ligand orbitals with σ symmetry are presently included in SIBFA-LF; an extension to π symmetry analogous to that of the LFMM force field described earlier remains to be implemented. E_{LFSE} of a d^n system is calculated from the orbital energies ε according to

$$E_{\mathrm{LFSE}} = -2\sum_{i=1}^{5}\varepsilon_i + \sum_{i=1}^{n}\rho_i\varepsilon_i + E_{\mathrm{wall}}, \tag{24}$$

where ρ_i is the occupation number of orbital i. The repulsive term E_{wall} is necessary to allow geometry optimization of a complex as the LFSE can become nonphysically large at very short range, leading to collapse. E_{wall} takes the form of an exponential with parameters c_{mul} and γ to be fitted for a given metal–ligand pair

$$E_{\mathrm{wall}} = \sum_l c_{\mathrm{mul}} \exp\left(-\gamma r_{\mathrm{ML}}\right). \tag{25}$$

While some of the terms included in the components of the SIBFA interaction energy are observable or can be obtained directly from ab initio calculations, others are parameters that must be fitted to ab initio reference data. Parametrization of metal–ligand complexes typically takes place in a mono-ligated complex involving the metal center and different types of ligand. Varying the M–L distance and performing RVS energy decomposition at each point allow the parametrization of the corresponding SIBFA energy terms as a function of distance. Validation can then take place by comparison with larger complexes and complexes involving different types of ligand. The large number of parameters to be fitted to account accurately for each term of the RVS decomposition means that parametrization of new metals or fragments can require a significant initial investment of time. Once parameters are available, however, they are generally more transferable than those

of simpler force fields and so are less likely to require refitting. For example, the polarization term of each fragment ensures that a single set of multipole moments in a methylene fragment is equally valid when used to build methanol and ethane.

2.3 VALBOND and VALBOND-TRANS

VALBOND, developed by Landis and coworkers [59–63], is based on valence bond theory, where hybrid orbital strength functions are used for the molecular mechanics. Following foundations laid by Pauling [64, 65] who examined chemical bonding from the perspective of valence bond theory, VALBOND aimed at correctly capturing bending potentials over a wide range of angular distortions which primarily determine the shape of molecules. VALBOND can describe both non-hypervalent and hypervalent molecules (not following the octet rule) [60] and transition metal complexes [62, 63] because the functional form for valence-angle distortions L1–M–L2 is suitable to also describe very large angular distortions. The formulation is based on generalized hybrid orbital strength functions. Given two equivalent sp^3 hybrid orbitals $\phi_1 = \frac{1}{2}\left(|1s\rangle + \sqrt{3}\,|p_z\rangle\right)$ and $\phi_2 = \frac{1}{2}[|1s\rangle + \sqrt{3}(\cos\,\alpha\,|p_z\rangle + \sin\alpha|p_x\rangle)]$, where the maximum value of φ_1 is along the z-axis and that of φ_2 is in the xz-plane and forms an angle α with φ_1, their strength S is given by the angular part which is $S = 2$ in both cases. The overlap between these two orbitals is $\Delta = \frac{1}{4}\left(1 + \sqrt{3}\,\cos\,\alpha\right)$. Pauling established that the decrease in S between two orbitals can be related to the overlap. Consequently, S represents a concentration of electron density in the bond-forming region, and S of hybrid orbitals has been interpreted as the bond-forming power of the orbitals. However, it was found that the correlation of S with bond dissociation energies is poor [14].

Nevertheless, the geometry-based hybrid orbital strength functions turned out to be useful to capture the angular parts of force fields. Therefore, VALBOND is used in conjunction with a conventional force field such as CHARMM, where the typical harmonic bending terms are replaced with a new parametrization. In fact, VALBOND was developed together with CHARMM [59]. The additional energy term is of the form

$$E_i = k_i\left(S_i^{\max} - S_i(\alpha_{ij})\right), \tag{26}$$

which arises for every ligand i. Here, k_i is an empirical scaling factor, $S_i^{\max}$ is the maximum strength for a particular hybrid orbital ($S^{\max} = 2$ for a sp^3 hybrid), and $S(\alpha_{ij})$ is the reduction in maximal strength due to the particular angular arrangement of the two hybrid orbitals involved (see above) on two different ligands i and j.

For two $sp^m d^n$ hybrid orbitals at an angle α, the expression for $S^{\max}$ is

$$S^{\max} = \sqrt{\frac{1}{1+m+n}}\left(1 + \sqrt{3m} + \sqrt{5n}\right) \tag{27}$$

and $S(\alpha)$ is in general given by

$$S(\alpha) = S^{\max}\sqrt{1 - \frac{1 - \sqrt{1 - \Delta^2}}{2}}. \tag{28}$$

The overlap Δ for two $sp^m d^n$ hybrid orbitals is

$$\Delta = \frac{1}{1 + m + n}\left(|1s\rangle + m\cos\alpha|p_z\rangle + \frac{n}{2}\left(3\cos^2\alpha - 1\right)|d_{z^2}\rangle\right). \tag{29}$$

Combining (26)–(29) constitutes the core of VALBOND.

For hypervalent molecules, one has to take into account that there are several resonance structures, each described by a weighting factor c_j, which depends on the geometry. For a 3-center/4-electron bond (such as in ClF_3), the total energy of the structure is the sum of three (formally equivalent) resonance structures, each of which are mixed ionic-covalent Lewis structures. Assigning a bond order of 1 to one particular CF bond with the two other CF bonds having bond order 1/2 (and cyclic permutation), the total energy of CF_3 is given by $E_{\text{tot}} = \sum_{j=1}^{3} c_j E_j$, where c_j are mixing coefficients which depend on the molecular geometry. One choice for these mixing coefficients is [60]

$$c_j = \frac{\prod_{i=1}^{hype}\cos^2\alpha_i}{\sum_{j=1}^{config}\prod_{i=1}^{hype}\cos^2\alpha_i}, \tag{30}$$

where the products run over all hypervalent angles i, and config stands for the number of resonance configurations. In general, the total energy is then given by

$$E_{\text{tot}} = \sum_j c_j E_j, \tag{31}$$

where the sum is over all resonance configurations j. For the energy expression E_j of a particular resonance configuration, the following form was suggested

$$E(\alpha) = \text{BOF} \times k_\alpha\left(1 - \Delta\,(\alpha + \pi)^2\right). \tag{32}$$

Here, BOF is the bond order factor, k_α is the VALBOND parameter (k for non-hypervalent bonds), Δ is given in (29) (for $sp^m d^n$ hybrid orbitals), and α is the bond angle. The BOF is the product of the formal bond orders of the two bonds described by the hybrid orbitals and standing at an angle α.

Despite these extensions, additional ingredients are necessary to capture electronic effects, such as the trans influence. One such generalization is VALBOND-TRANS [66]. The purpose of this additional development is to capture electronic effects related to the structural trans effect. Quadratic planar complexes, especially

Pt(II) metal complexes, are known to exhibit a structural trans effect. In octahedral complexes, trans effects can also occur, even if these effects are less pronounced [67]. The trans effect is attributed to electronic effects and is defined as "the effect of a coordinated group on rate of substitution reactions of ligands trans to itself" [68]. One can distinguish between an energetic (or kinetic) trans effect and a structural trans effect in an arrangement L1–M–L2. Here, L1 is trans to L2. The energetic trans effect (not considered in VT) refers to a bond weakening of the M–L2 bond depending on the chemical identity of ligand L1. Contrary to this, the structural trans effect (or influence) reports on bond length changes in M–L2 depending on L1 [69].

The key equation in VALBOND for hypervalent compounds is (32). For a 3-center/4-electron bond, it describes the bending energy as the overlap between one orbital and another orbital shifted by 180°. This term favors linear geometries in hypervalent bonds because it is at a minimum for $\alpha = 180°$. Because the trans influence also acts along hypervalent bonds and is expected to be maximal at linear geometries, a natural place to include additional electronic effects is the term $\Delta(\alpha + \pi) = 1$. This is done by reweighting the energy depending on the chemical identity of ligands L1 and L2 trans to each other in the motif L1–M–L2

$$E_{\text{trans}} = \sum_{\text{trans}} p_{\text{AB}} \left(\Delta(\alpha + \pi)^2 \right). \tag{33}$$

Here, A and B stand for the chemical identity of the atoms of L1 and L2, respectively, bonding to the metal M; p_{AB} is a parameter for the structural trans effect, which depends on the atom types involved and the metal; and α is the L1–M–L2 angle [66]. For a perfect octahedron, this expression is simplified to

$$E_{\text{trans}} = \sum_{\text{trans}} p_{\text{AB}}. \tag{34}$$

To consider the structural trans influence, one has to determine the bond lengths

$$r_{\text{A(B)}} = r_{\text{A}}^0 (1 + s_{\text{A}} \times i_{\text{B}}/100), \tag{35}$$

where $r_{\text{A(B)}}$ is the equilibrium bond length A–M which has atom B trans to it. r_{A}^0 is the unperturbed bond length A–M, i_{B} is the bond lengthening intensity of atom type B, and S_{A} is the bond lengthening sensitivity of atom type A. The trans influence and, therefore, the relative change in the bond length $r_{\text{A(B)}}$ are captured in VALBOND-TRANS as [66]

$$r_{\text{A(B)}} = r_{\text{A}}^0 \left(1 + s_{\text{A}} \times \Delta(\alpha + \pi)^2 \cdot \ i_{\text{B}}/100 \right). \tag{36}$$

2.4 Combination of VALBOND-TRANS with MMPT

One advantage of force field methods is their extensibility. To model a chemically complicated compound, different and separately developed force field methods can be combined. A more familiar example might be the combined quantum mechanics/molecular mechanics (QM/MM) approach [70], which treats a localized region (usually where the chemical reactions occur) by QM methods and the rest of the system by MM force fields. Similarly, we can combine VALBOND with another force field developed in our group, molecular mechanics with proton transfer (MMPT) [71, 72], to study the transition metal complexes whose ligands interact via strong hydrogen bonds. The system can be partitioned into regions treated by VALBOND or MMPT or conventional CHARMM force field, as we will discuss in detail in the application section. Dealing with the interactions across the boundary of different MM regions is relatively simple since force field is additive, while in QM/MM methods the correct description of the boundary region still remains a technical challenge [73].

A detailed account of MMPT has been given in [72]. Briefly, MMPT uses parametrized three-dimensional potential energy surfaces (PES) $V(R, \rho, \theta)$ fitted to high-level ab initio calculations (MP2/6-311++G(d,p)) of prototype proton transfer systems (H_3N–H^+···NH_3, H_2O–H^+···OH_2 and H_3N–H^+···OH_2) to describe the interactions within a general DH–A motif, where D is the donor, H is the hydrogen, and A is the acceptor atom. R is the distance between the donor and the acceptor, ρ is the relative position of H for a particular value of R, and θ is the angle between vectors $\overrightarrow{DA}$ and $\overrightarrow{DH}$. The relationship between ρ and the D–H distance r is given by

$$\rho = (r - r_{\min})/(R - 2r_{\min}), \tag{37}$$

where $r_{\min} = 0.8$ Å is in principle arbitrary but should be sufficiently small to cover the shortest D–A separations. Depending on the position of the transferring H-atom (DH–A or D–HA), bonded interactions on the donor and acceptor side are switched on and off. And by PES morphing [74] through coordinate transformations, MMPT is capable of describing topologically similar but energetically different hydrogen-bonding motifs in an accurate and concise way. VALBOND and MMPT have both been implemented into CHARMM [75]. The implementation has been made in such a way that VALBOND is by default applied to all the atoms and MMPT is applied only to predefined atoms.

3 Applications

3.1 *Refining Force Field Parameters in VALBOND TRANS: Application to an Octahedral Iridium-PHOX Catalyst*

DFT has, over the past decade, emerged as a convenient and versatile computational method. It has been used successfully to obtain a wide range of data such as thermochemistry, molecular structures, force field parameters, vibrational frequencies, nuclear magnetic resonance and electron spin resonance characteristics, UV spectra, dipole moments, transition-state structures, and activation barriers [76]. DFT is also used to provide reference values for the VALBOND-TRANS force field. In this work, DFT calculations were carried out using the B3LYP functional [1, 2] with the all-electron 6-31G(d,p) basis set for C, H, N, O, and P atoms, and a LANL2DZ ECP [77] for Ir, Pt, and Cl atoms. All electronic structure calculations were carried out using the Gaussian03 suite of programs [78] with the grid=ultrafine option.

In the following, the VALBOND-TRANS force field is parametrized for model octahedral complexes of Ir, with the aim to best capture relative energies calculated from DFT for different diastereomers. The (re-)parametrization of VALBOND-TRANS is important for successful use in further atomistic simulations. The fitting procedure can be conveniently carried out by using a recent combination of CHARMM and the I-NoLLS fitting environment [79, 80]. This parameter optimization environment can carry out interactive nonlinear least-square fittings to determine model parameters for a wide variety of applications.

Here, a first optimization of the van der Waals parameters of an octahedral iridium(III)-PHOX catalyst with a triphenylposphate coordinated group (see Fig. 1) is described in some more detail. Starting from standard vdW parameters $R_{\min,i}$ and ε_i and nuclear charges q_i, several optimization cycles are carried out to better reproduce the relative energetics of 20 diastereomers of the test compound. The relative energies from B3LYP/6-31G(d,p) calculations span a range of 21 kcal/mol. Using these energies as the target data, the vdW parameters are iteratively improved. Figure 2 compares the initial RMSD between the reference data (DFT) and VALBOND-TRANS without (green squares) and with optimized vdW parameters (blue circles). It decreases from 7.37 to 3.74 kcal/mol, which is an improvement of 50%. A linear regression gives a correlation coefficient of 0.87 and 0.92, respectively. The most significant change concerns ε_i for the phosphorus atom, which decreases from −0.585 to −1.378 kcal/mol. Noticeable changes also occur for the vdW radii of N (from 1.85 to 1.06 Å), Ir (from 1.91 to 2.75 Å), and P (from 2.15 to 1.53 Å).

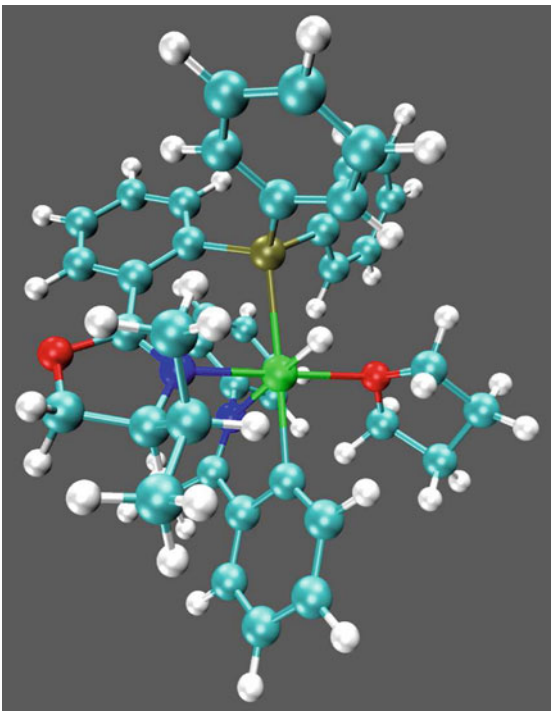

Fig. 1 One diastereomer of the octahedral Ir(III)–metal complex. Color codes are as follows: *light green*: Ir, *light blue*: C, *dark green*: P, *red*: N, *dark blue*: O, *white*: H

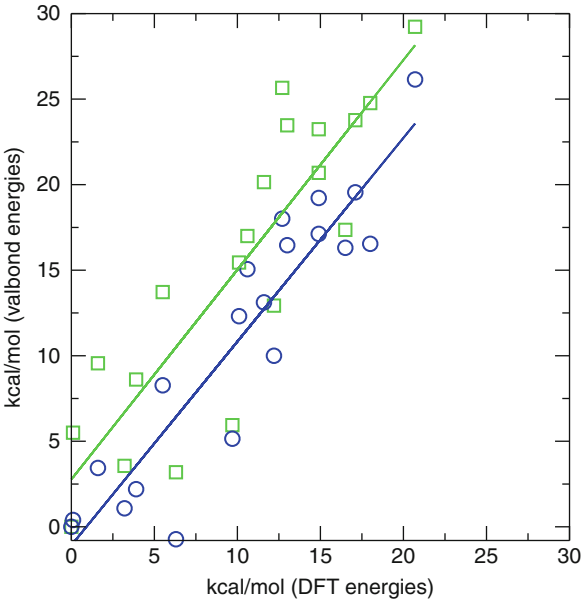

Fig. 2 Energies of all diastereomers of the Ir(III)–metal complex, using unoptimized Lennard-Jones parameters (*green squares*) and fitted Lennard-Jones parameters (*blue cycles*), both with unoptimized Mulliken charges. All energies (kcal/mol) are relative to that of complex 3

3.2 *Energetics and Dynamics of a Hydrogen-Bonded Bidentate Catalyst*

Bidentate ligands are important for controlling selectivity in homogeneous catalysis, but their synthesis is difficult and rational design is usually impossible. In 2003, Breit et al. proposed a new approach for generating bidentate ligands by self-assembly of monodentate ligands via complementary hydrogen-bonding interactions [81]. For example, the self-assembly of 6-diphenylhposphanyl-pyridone (6-DPPon) in the presence of a transition metal such as platinum(II) or rhodium(I) can provide high activity and regioselectivity in the hydroformylation of terminal alkenes [81–83]. In this subsection, we study the energetics and dynamics of *cis*-Pt[Cl_2(6-DPPon)$_2$] [81], a hydrogen-bonded catalyst, with an MM force field.

The Force Field: As illustrated in Fig. 3, the force field for Pt[Cl_2(6-DPPon)$_2$] is decomposed into three parts: the metal center Pt and the ligand atoms P and Cl that are treated with VALBOND; the double proton transfer (DPT) motifs N–H–N and O–H–O which are described by MMPT potentials; and the remainder of the molecule for which the conventional CHARMM force field is used.

The parameters for VALBOND are directly taken from the literature [59, 62] and the corresponding supplementary materials. Force field parameters for MMPT are based on our previous study of 2-pyridone·2-hydroxypyridine (2PY2HP) dimer [72]. Since the DPT motif in the two systems is topologically similar, the MMPT PESs of 2PY2HP are regarded as the zeroth-order potentials, and the following PES morphing [74] is applied

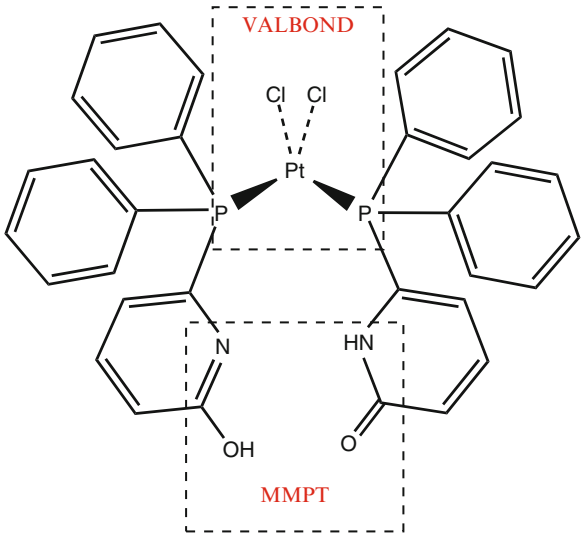

Fig. 3 Pt[Cl_2(6-DPPon)$_2$], and the force field decomposition

$$V^{\mathrm{NHN}}(R',\,\rho',\,\theta') = 0.75 \times V_0^{\mathrm{NHN}}(R - 0.08,\,\rho + 0.235, 0.85\theta)$$
$$V^{\mathrm{OHO}}(R',\,\rho',\,\theta') = 0.75 \times V_0^{\mathrm{OHO}}(R + 0.03,\,\rho - 0.210, 0.70\theta) \tag{38}$$

to generate the PES—and thus the corresponding MMPT parameters—for the Pt complex in this study. The CHARMM22 parameter set [4] is used for all other force field terms required. When CHARMM parameters were missing, those from analogous CHARMM atom types are used, as was done in the previous work [66]. The Lennard-Jones parameters for Pt and Cl atoms are taken from [84], and all the atomic partial charges are determined from natural population analysis (NPA) [85].

The efficiency of force field approaches allows also to perform calculations in explicit solvent. To demonstrate this, we have solvated the Pt[Cl_2(6-DPPon)$_2$] complex in deuterochloroform and carried out MD simulations. The force field parameters for $CDCl_3$ are determined by combining ab initio calculation results at the MP2/6-311++G** level and suggested values from the literature [86, 87].

Validation of the Force Field: As a validation of the MM force field, equilibrium structures of *cis*-Pt[Cl_2(6-DPPPon)$_2$] are determined by different methods and compared in Fig. 4. Starting from the experimental X-ray structure [81], conjugate gradient minimization with CHARMM is used to further relax it, and the DFT structure is generated by full optimization at the B3LYP/6-31G**/LANL2DZ level. The three structures overlap with each other very well (see bond lengths and angles in Table 2). The distances between the platinum center and ligand atoms (P and Cl) are well reproduced by the MM force field, while the P–Pt–P angle in the MM structure differs by 10° and 18° with the X-ray and DFT structures, respectively. This is related to the predefined hybridization of the Pt atom in VALBOND force field, and can be optimized by manually assigning a different sp^{m}d^n hybridization.

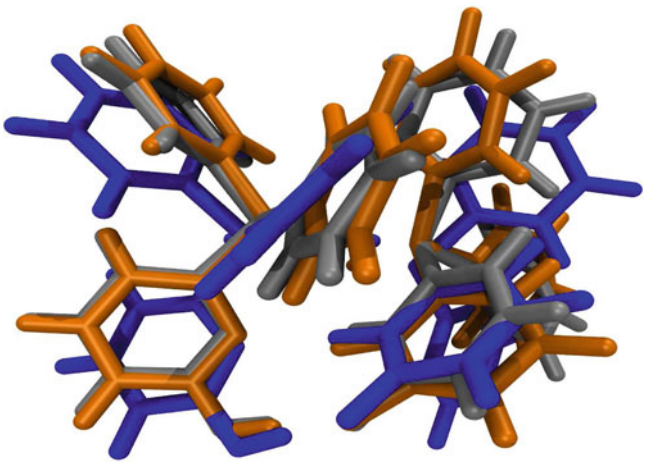

Fig. 4 Superposition of the X-ray structure (*silver*), DFT equilibrium structure (*blue*), and MM structure (*orange*) of *cis*-Pt[Cl_2(6-DPPon)$_2$]

Table 2 Comparison of selected bond lengths and angles from structures determined by X-ray crystallography [81], MM force field optimization, and DFT optimization

Geometry	X-ray	DFT	MM
N–N	3.070	2.966	2.967
N–H	0.84	1.033	1.033
∠N–H–N	136.9	156.3	155.5
O–O	2.684	2.631	2.632
O–H	0.86	1.003	1.004
∠O–H–O	164.3	173.3	177.7
Pt–P[a]	2.247	2.310	2.312
∠P–Pt–P	97.6	105.5	87.6
Pt–Cl[a]	2.338	2.462	2.438
P–C[a]	1.825	1.841	1.872

[a]Average values

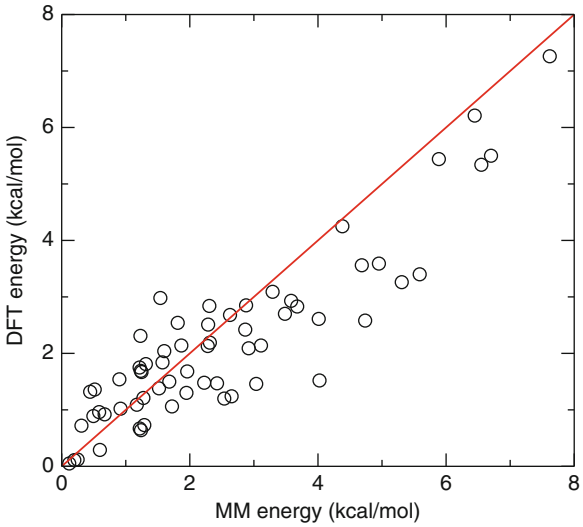

Fig. 5 Comparison of energies calculated by MM force field and DFT method

Besides the equilibrium structure, energies at different hydrogen-bonding situations are also compared. DFT energy calculations are performed by fixing the N–N distance R_{NN}, the O–O distance R_{OO}, the N–H bond length r_{NH}, and the O–H bond length r_{OH} while fully relaxing other degrees of freedom. Such computations have been carried out on a regular grid, giving 63 single-point DFT energies in total. The same constrained minimizations were done with the MM force field. These two sets of energies are compared in Fig. 5. The correlation coefficient between the MM and DFT energies is 0.90, and the mean absolute error (MAE) equals 0.68 kcal/mol. Considering the error of DFT energy calculations which is ≈0.5 kcal/mol, the performance of MM force field is acceptable.

It is worth pointing out that no fitting procedure is performed in this work. The MMPT force field parameters are generated by mapping those of a previously

studied system 2PY2HP to new ones. The PES morphing presented here is heuristic, and a more sophisticated morphing strategy is currently under investigation. Fitting with a CHARMM/I-Nolls interface [80] is also a possible if sufficient experimental data or high-level ab initio calculation results are available.

Molecular Dynamics Simulations: With rapid evaluation of energies and gradients, molecular dynamics (MD) simulations can be carried out. For MD simulations in the gas phase, the complex was first heated to 300 K by 6,000 steps and equilibrated at that temperature for 100 ps. Then, a 5-ns NVE trajectory was generated by free dynamics. The time step was 0.1 fs to follow the fast proton motions. For simulations in explicit solvent, a 46.0 Å × 46.0 Å × 40.9 Å box of $CDCl_3$ was first generated with a density of 1.50 g/cm^3. The Pt[Cl_2(6-DPPon)$_2$] complex was then solvated and periodic boundary conditions were applied. A cutoff of 12 Å was applied to the shifted electrostatic and switched van der Waals interactions. Before 1-ns free dynamics simulations, the system was heated to 300 K and then equilibrated for 10^5 time steps.

One of the essential issues in using nonstandard force fields is whether MD simulations carried out with them conserve total energy. The energy fluctuations $\Delta E(t) = E(t) - \langle E \rangle$ along the 5-ns MD trajectory are shown in Fig. 6. The probability histogram of ΔE is near-Gaussian, with a full width at half maximum (FWHM) of 0.005 kcal/mol. For the 1-ns MD simulation in $CDCl_3$ solvation, the fluctuation of total energies is also small and the FWHM equals 0.02 kcal/mol. Thus, the total energies in NVE simulations are conserved on the nanosecond timescale, which ensures that forces are calculated correctly and that further analysis of the MD trajectories yields meaningful results.

It will be interesting to use this parametrization to further investigate infrared and NMR spectra. These applications will require conformational sampling of the metal complex at finite temperature, which will provide useful starting points for more detailed investigations at the DFT level. For example, an accurate assessment of the temperature-dependent ^{1}H-NMR spectrum of Pt[Cl_2(6-DPPon)$_2$] can only be achieved by combining our MM force field and DFT calculations. Such a study is currently in progress.

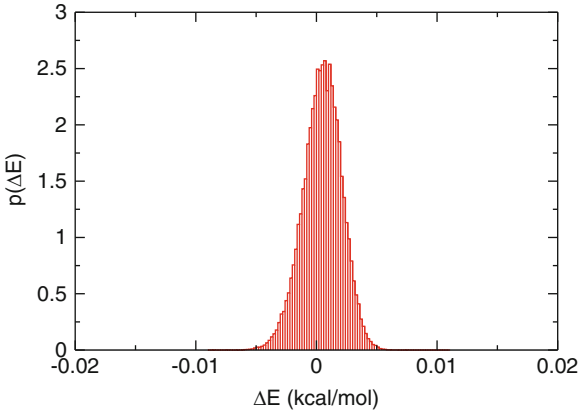

Fig. 6 The fluctuations of total energy ($\Delta E = E - \langle E \rangle$) sampled from a 5-ns molecular dynamics trajectory for *cis*-Pt [Cl_2(6-DPPon)$_2$] in gas phase at 300 K

4 Outlook

This outlook summarizes some new and expected future developments in investigating organometallic chemistry using force field-based techniques.

For the particular case of VALBOND-TRANS, a more comprehensive fitting of an integrated force field is an obvious next step. Until now it was demonstrated that inclusion of electronic effects such as the trans-influence is possible and leads to quantitatively meaningful results when compared with reference DFT calculations. However, for a dedicated force field, all terms (including the bonded ones) need to be fitted. An important question will be how transferable the resulting FF parameters are for the standard chemical atom types (H, C, N, O) between complexes with different transition metals, or whether independent parametrizations are required for different metals and different oxidation states.

The combination of largely independent but mutually beneficial techniques such as VALBOND-TRANS and MMPT as shown in Sect. 3.2 will open up new possibilities in organometallic chemistry. Such extensions can also be envisaged between VALBOND-TRANS and adiabatic reactive MD (ARMD) [88], which will allow reactions involving TMs to be followed explicitly. A prerequisite for such applications is to more routinely adjust force field parameters for particular chemistries.

Approaches discussed in this chapter address the problem of describing TM complexes from two largely different perspectives. Either one starts from a force field and seeks to suitably extend its range of applicability by adding (or integrating) new terms which can describe electronic degrees of freedom (LFMM, VALBOND). Alternatively, one can start from an energy expression and decompose it into terms that can be parametrized. Ultimately, one will be interested not only in carrying out energy evaluations but also in sampling configurational space using such an energy expression. Thus, either Monte Carlo or MD simulations should be possible with such a force field. For VALBOND-TRANS dynamics, the possibility to carry out MD simulations has been demonstrated here, and LFMM has recently been applied to study the dynamics of tyrosinase (a copper-containing protein) [89]. As analytical derivatives for the different terms of the SIBFA interaction energy are not yet fully implemented, the application of SIBFA over recent years has primarily been to the energetic analysis of interactions in biomolecules that are too large to be examined with full ab initio calculations [43, 44, 90, 91]. The envisaged extension of SIBFA to molecular dynamics simulations would allow exploration of an accurate and detailed free energy surface, and remains an important goal. The ability to model metal ion centers accurately in enzyme active sites in energy minimizations and single-point calculations, however, makes SIBFA a useful tool where meaningful analysis of protein–ligand-binding interactions using a classical, nonpolarizable force field is challenging, and where the number of atoms is too large to successfully employ ab initio techniques. The polarization energy in systems with charged metal ions in particular contributes strongly to the total interaction energy [44]. Some recent applications include

modeling of binding energies of different low-energy ligand conformations in protein-active sites in docking studies [90, 91], examining the role of polarizable water molecules in ligand binding [43], and modeling of the formation of complexes that comprise ligand field effects [38].

A major issue remains to incorporate polarization effects in conventional force fields. Polarization can be divided into two important contributions. *Intramolecular polarization*, the response of a molecule's electron density to changes in molecular conformation, can be important in calculating certain sensitive dynamic properties. Modeling of bond vibrational responses to local electric fields in MD simulations provides one such example [92–94]. This form of polarization is currently missing in many force fields and is only partially present even in detailed potentials such as SIBFA, which have focused on an accurate representation of the second, *intermolecular polarization*. Intermolecular polarization describes the response of the electron density of one molecule to the electric field generated by its nonbonded neighbors. As the intermolecular polarization energy is a function of the external electric field, which originates from multipole moments of surrounding moieties which are themselves polarizable, a self-consistent procedure is necessary to achieve very accurate results. Successful incorporation of both inter- and intramolecular polarization within a single force field would allow fully polarizable molecular dynamics simulations, which may offer an important increase in accuracy for detailed applications in charged or polar environments.

Acknowledgments This work is supported by the Schweizerischer Nationalfonds. The authors acknowledge stimulating discussions with Profs. N. Gresh and J.-P. Piquemal.

References

1. Lee C, Yang R, Parr WG (1988) Development of the Colle-Salvetti correlation-energy formula into a functional of the electron density. Phys Rev B 37:785
2. Becke AD (1993) Density-functional thermochemistry. III. The role of exact exchange. J Chem Phys 98:5648
3. Weiner SJ, Kollman PA, Case DA, Singh U, Ghio C, Alagona G, Profeta S Jr, Weiner P (1984) A new force-field for molecular mechanical simulation of nucleic-acids and proteins. J Am Chem Soc 106:765
4. MacKerell JAD, Bashford D, Bellott M, Dunbrack JRL, Evanseck JD, Field MJ, Fischer S, Gao J, Guo H, Ha S, Joseph-McCarthy D, Kuchnir L, Kuczera K, Lau FTK, Mattos C, Michnick S, Ngo T, Nguyen DT, Prodhom B, Reiher I, Roux B, Schlenkrich M, Smith JC, Stote R, Straub J, Watanabe M, Wiorkiewicz-Kuczera J, Yin D, Karplus M (1998) All atom empirical potential for molecular modeling and dynamics studies of proteins. J Phys Chem B 102:3586
5. Jorgensen WL, Tirado-Rives J (1657) The OPLS potential functions for proteins–energy minimizations for crystals of cyclic-peptides and crambin. J Am Chem Soc 110
6. Comba P (1993) The relation between ligand structures, coordination stereochemistry, and electronic and thermodynamic properties. Coord Chem Rev 123:1
7. Landis CR, Root DM, Cleveland T (1995) Reviews in computational chemistry. Rev Comput Chem 6:73

8. Zimmer M (1995) Bioinorganic molecular mechanics. Chem Rev 95:2629
9. London F (1929) Quantum mechanical interpretation of the process of activation. Z Elektrochem 35:552
10. Eyring H, Polanyi M (1931) Concerning simple gas reactions. Z Phys Chem Abt B 12:279
11. Sato S (1955) On a new method of drawing the potential energy surface. J Chem Phys 23:592
12. Sato S (1955) Potential energy surface of the system of three atoms. J Chem Phys 23:2465
13. Ellison FO (1963) A method of diatomics in molecules. 1. General theory and application to H2O. J Am Chem Soc 85:3540
14. Pauling L (1960) The nature of the chemical bond. Cornell University Press, Ithaca, NY
15. Pauling L (1932) The nature of the chemical bond. IV. The energy of single bonds and the relative electronegativity of atoms. J Am Chem Soc 54:3570
16. Johnston HS, Parr C (1963) Activation energies from bond energies. I. Hydrogen transfer reactions. J Am Chem Soc 85:2544
17. van Duin ACT, Dasgupta S, Lorant F, Goddard WA III (2001) ReaxFF: a reactive force field for hydrocarbons. J Phys Chem A 105:9396
18. Lifson S, Warshel A (1968) Consistent force field fpr calculations of conformations vibrational spectra and enthalpies of cycloalkane and n-alkane molecules. J Chem Phys 49:5116
19. Levitt M, Lifson S (1969) Refinement of protein conformations using a macromolecular energy minimization procedure. J Mol Biol 46:269
20. Hwang MJ, Stockfisch TP, Hagler AT (1994) Derivation of class II force fields: 2. Derivation and characterization of a class II force field, CFF93, for the alkyl functional group and alkane molecules. J Am Chem Soc 116:2515
21. Maple JR, Hwang MJ, Stockfisch TP, Dinur U, Waldman M, Ewig CS, Hagler AT (1994) Derivation of class-II force-fields: 1. Methodology and quantum force-field for the alkyl functional-group and alkane molecules. J Comput Chem 15:162
22. Brooks B, Bruccoleri R, Olafson B, States D, Swaminathan S, Karplus M (1983) CHARMM: A program for macromolecular energy, minimization, and dynamics calculations. J Comput Chem 4:18
23. Hermans J, Berendsen HJC, van Gunsteren WF, Postma JPM (1984) A consistent empirical potential for water-protein interactions. Biopolymers 23:1513
24. Deeth R, Anastasi A, Diedrich C, Randell K (2009) Molecular modelling for transition metal complexes: dealing with d-electron effects. Coord Chem Rev 253:795
25. Figgis BN, Hitchman MA (2000) Ligand field theory and its applications. Wiley-VCH, New York
26. Burton VJ, Deeth RJ, Kemp CM, Gilbert PJ (1995) Molecular mechanics for coordination complexes: the impact of adding d-electron stabilization energies. J Am Chem Soc 117:8407
27. Deeth RJ, Fey N, Deeth RJ, Fey N (2004) A molecular mechanics study of copper(II)-catalyzed asymmetric Diels-Alder reactions. Organometallics 23:1042
28. Deeth RJ, Fey N, Williams-Hubbard B (2005) DommiMOE: an implementation of ligand field molecular mechanics in the molecular operating environment. J Comput Chem 26:123
29. Deeth RJ, Hearnshaw LJA (2005) Molecular modelling for coordination compounds: Cu(II)-amine complexes. Dalton Trans 22:3638–3645
30. Deeth RJ (2008) General molecular mechanics method for transition metal carboxylates and its application to the multiple coordination modes in mono- and dinuclear Mn(II) complexes. Inorg Chem 47:6711
31. Deeth RJ, Randell K (2008) Ligand field stabilization and activation energies revisited: molecular modeling of the thermodynamic and kinetic properties of divalent, first-row aqua complexes. Inorg Chem 47:7377
32. Deeth RJ (2007) Comprehensive molecular mechanics model for oxidized type I copper proteins: active site structures, strain energies, and entatic bulging. Inorg Chem 46:4492
33. Schaeffer CE, Jorgensen CK (1965) The angular overlap model, an attempt to revive the ligand field approaches. Mol Phys 9:401

34. Larsen E, Mar GNL (1974) The angular overlap model. How to use it and why. J Chem Educ 51:633
35. Schaeffer CE (1968) A perturbation representation of weak covalent bonding. Struct Bond 5:68
36. Halgren TA (1998) Merck molecular force field. I. Basis, form, scope, parameterization, and performance of MMFF94. J Comput Chem 17:490
37. Gresh N, Claverie P, Pullman A (1984) Theoretical studies of molecular conformation. Derivation of an additive procedure for the computation of intramolecular interaction energies. Comparison with ab initio SCF computations. Theor Chim Acta 66:1
38. Piquemal J-P, Williams-Hubbard B, Fey N, Deeth RJ, Gresh N, Giessner-Prettre C (2003) Inclusion of the ligand field contribution in a polarizable molecular mechanics: SIBFA-LF. J Comput Chem 24:1963
39. Gresh N (1995) Energetics of Zn binding to a series of biologically relevant ligands: a molecular mechanics investigation grounded on ab initio self-consistent field supermolecule calculations. J Comput Chem 16:856
40. Piquemal J-P, Gresh N, Giessner-Prettre C (2003) Improved formulas for the calculation of the electrostatic contribution to the intermolecular interaction energy from multipolar expansion of the electronic distribution. J Phys Chem A 107:10353
41. Gresh N, Policar C, Giessner-Prettre C (2002) Modeling copper(I) complexes: SIBFA molecular mechanics versus *ab initio* energetics and geometrical arrangements. J Phys Chem A 106:5660
42. Gresh N, Piquemal J-P, Krauss M (2005) Representation of Zn(II) complexes in polarizable molecular mechanics. Further refinements of the electrostatic and short-range contributions. Comparison with ab initio computations. J Comput Chem 26:1113
43. de Courcy B, Piquemal J-P, Garbay C, Gresh N (2010) Polarizable water molecules in ligand-macromolecule recognition. Impact on the relative affinities of competing pyrrolopyrimidine inhibitors for FAK kinase. J Am Chem Soc 132:3312
44. de Courcy B, Piquemal J-P, Gresh N (2008) Energy analysis of Zn polycoordination in a metalloprotein environment and of the role of a neighboring aromatic residue. What is the impact of polarization? J Chem Theor Comput 4:1659
45. Stevens WJ, Fink W, Stevens WJ, Fink W (1987) Frozen fragment reduced variational space analysis of hydrogen-bonding interactions—application to the water dimer. Chem Phys Lett 139:15
46. Piquemal J-P, Chevreau H, Gresh N (2007) Toward a separate reproduction of the contributions to the Hartree-Fock and DFT intermolecular interaction energies by polarizable molecular mechanics with the SIBFA potential. J Chem Theor Comput 3:824
47. Vigne-Maeder F, Claverie P (1988) The exact multipolar part of a molecular charge-distribution and its simplified representations. J Chem Phys 88:4934
48. Popelier PLA (2000) Atoms in molecules: an introduction. Pearson Education, London
49. Stone AJ (1996) The theory of intermolecular forces. Clarendon, Oxford
50. Becke AD, Edgecombe KE (1990) A simple measure of electron localization in atomic and molecular systems. J Chem Phys 92:5397
51. Murrell JN, Teixeiras-Dias JJN (1970) The dependence of exchange on orbital overlap. Mol Phys 19:521
52. Gresh N (1997) Model, multiply hydrogen-bonded water oligomers (N=3-20). How closely can a separable, ab initio-grounded molecular mechanics procedure reproduce the results of supermolecule quantum chemical computations? J Phys Chem A 101:8680
53. Gresh N, Claverie P, Pullman A (1986) Intermolecular interactions: elaboration on an additive procedure including an explicit charge-transfer contribution. Int J Quant Chem 29:101
54. Gresh N (1995) Energetics of Zn^{2+} binding to a series of biologically relevant ligands: a molecular mechanics investigation grounded on ab initio self-consistent field supermolecular computations. J Comput Chem 16:856

55. Murrell JN, Randic M, Williams DR (1965) The theory of intermolecular forces in the region of small orbital overlap. Proc R Soc Lond 284:566
56. Gresh N, Claverie P, Pullman A (1985) Cation-ligand interactions: reproduction of extended basis set *ab initio* SCF computations by the SIBFA 2 additive procedure. Int J Quant Chem 28:757
57. Gresh N, Claverie P, Pullman A (1982) Computations of intermolecular interactions: expansion of a charge-transfer energy contribution in the framework of an additive procedure. Applications to hydrogen-bonded systems. Int J Quant Chem 22:199
58. Woodley SM, Battle PD, Catlow CRA, Gale JD (2001) Development of a new interatomic potential for the modeling of ligand field effects. J Phys Chem B 105:6824
59. Root DM, Landis CR, Cleveland T (1993) Valence bond concepts applied to the molecular mechanics description of molecular shapes. 1. Application to nonhypervalent molecules of the p-block. J Am Chem Soc 115:4201
60. Cleveland T, Landis CG (1996) Valence bond concepts applied to the molecular mechanics description of molecular shapes. 2. applications to hypervalent molecules of the p-block. J Am Chem Soc 118:6020
61. Landis CR, Firman TK, Root DM, Cleveland T (1998) A valence bond perspective on the molecular shapes of simple metal alkyls and hydrides. J Am Chem Soc 120:1842
62. Landis CR, Cleveland T, Firman TK (1998) Valence bond concepts applied to the molecular mechanics description of molecular shapes. 3. Applications to transition metal alkyls and hydrides. J Am Chem Soc 120:2641
63. Firman TK, Landis CR (2001) Valence bond concepts applied to the molecular mechanics description of molecular shapes. 4. Transition metals with pi-bonds. J Am Chem Soc 123:11728
64. Pauling L (1928) The shared-electron chemical bond. Proc Natl Acad Sci USA 14:359
65. Pauling L (1931) The nature of the chemical bond. Application of results obtained from the quantum mechanics and from a theory of paramagnetic susceptibility to the structure of molecules. J Am Chem Soc 53:1367
66. Tubert-Brohman I, Schmid M, Meuwly M (2009) A molecular mechanics force field for octahedral organometallic compounds with inclusion of the trans influence. J Chem Theor Comput 5:530
67. Quagliano JV, Schubert L (1952) The trans effect in complex inorganic compounds. Chem Rev 50:201
68. Coe BJ, Glenwright SJ (2000) Trans-effects in octahedral transition metal complexes. Coord Chem Rev 203:5
69. Anderson KM, Orpen AG (2001) On the relative magnitudes of cis and trans influences in metal complexes. Chem Commun 2682–2683
70. Warshel A, Levitt M (1976) Theoretical studies of enzymic reactions: dielectric, electrostatic and steric stabilization of the carbonium ion in the reaction of lysozyme. J Mol Biol 103:227
71. Lammers S, Meuwly M (2007) On the relationship between infrared spectra of shared protons in different chemical environments: a comparison of protonated diglyme and protonated water dimer. J Phys Chem A 111:1638
72. Lammers S, Lutz S, Meuwly M (2008) Reactive force fields for proton transfer dynamics. J Comput Chem 29:1048
73. Lin H, Truhlar DG (2007) QM/MM: what have we learned, where are we, and where do we go from here? Theor Chim Acta 117:185
74. Meuwly M, Hutson J (1999) Morphing ab initio potentials: a systematic study of Ne-HF. J Chem Phys 110:8338
75. Brooks BR, Bruccoleri RE, Olafson BD, States DJ, Swaminathan S, Karplus M (1983) CHARMM: a program for macromolecular energy, minimization and dynamics calculations. J Comput Chem 4:187
76. Ziegler T (1991) Approximate density functional theory as a practical tool in molecular energetics and dynamics. Chem Rev 91:651

77. Hay PJ, Wadt WR (1985) Ab initio effective core potential for molecular calculation. J Chem Phys 82:270
78. Frisch MJ, Trucks GW, Schlegel HB, Scuseria GE, Robb MA, Cheeseman JR, Montgomery JJA, Vreven T, Kudin KN, Burant JC, Millam JM, Iyengar SS, Tomasi J, Barone V, Mennucci B, Cossi M, Scalmani G, Rega N, Petersson GA, Nakatsuji H, Hada M, Ehara M, Toyota K, Fukuda R, Hasegawa J, Ishida M, Nakajima T, Honda Y, Kitao O, Nakai H, Klene M, Li X, Knox JE, Hratchian HP, Cross JB, Bakken V, Adamo C, Jaramillo J, Gomperts R, Stratmann RE, Yazyev O, Austin AJ, Cammi R, Pomelli C, Ochterski JW, Ayala PY, Morokuma K, Voth GA, Salvador P, Dannenberg JJ, Zakrzewski VG, Dapprich S, Daniels AD, Strain MC, Farkas O, Malick DK, Rabuck AD, Raghavachari K, Foresman JB, Ortiz JV, Cui Q, Baboul AG, Clifford S, Cioslowski J, Stefanov BB, Liu G, Liashenko A, Piskorz P, Komaromi I, Martin RL, Fox DJ, Keith T, Al-Laham MA, Peng CY, Nanayakkara A, Challacombe M, Gill PMW, Johnson B, Chen W, Wong MW, Gonzalez C, Pople JA (2004) Gaussian 03, Revision C.02. Gaussian Inc, Wallingford, CT
79. Law MM, Hutson JM (1997) I-NoLLS: a program for interactive nonlinear least-square fitting of the parameters of physical models. Comp Phys Commun 102:252
80. Devereux M, Meuwly M (2010) Force field optimization using dynamics and ensemble-averaged data: vibrational spectra and relaxation in bound MbCO. J Chem Inf Model 50:349
81. Breit B, Seiche W (2003) Hydrogen bonding as a construction element for bidentate donor ligands in homogeneous catalysis: regioselective hydroformylation of terminal alkenes. J Am Chem Soc 125:6608
82. Seiche W, Schuschkowski A, Breit B (2005) Bidentate ligands by self-assembly through hydrogen bonding: a general room temperature/ambient pressure regioselective hydroformylation of terminal alkenes. Adv Synth Catal 347:1488
83. Chevallier F, Breit B (2006) Self-assembled bidentate ligands for Ru-catalyzed anti-Markovnikov hydration of terminal alkynes. Angew Chem Int 45:1599
84. Lienke A, Klatt G, Robinson DJ, Koch KR, Naidoo KJ (2001) Modeling platinum group metal complexes in aqueous solution. Inorg Chem 40:2352
85. Glendening ED, Reed AE, Carpenter JE, Weinhold F NBO Version 3.1
86. Fox T, Kollman PA (1998) Application of the RESP methodology in the parametrization of organic solvents. J Phys Chem B 102:8070
87. Kab G, Schroder C, Schwarzer D (2002) Intramolecular vibrational redistribution and energy relaxation in solution: a molecular dynamics approach. PCCP 4:271
88. Danielsson J, Meuwly M (2008) Atomistic simulation of adiabatic reactive processes based on multi-state potential energy surfaces. J Chem Theor Comput 4:1083
89. Deeth RJ, Diedrich C (2010) Structural and mechanistic insights into the oxy form of tyrosinase from molecular dynamics simulations. J Biol Inorg Chem 15:117
90. Gresh N, Audiffren N, Piquemal JP, de Ruyck J, Ledecq M, Wouters J (2010) Analysis of the interactions taking place in the recognition site of a bimetallic Mg(II)-Zn(II) enzyme, isopentenyl diphosphate isomerase. A parallel quantum-chemical and polarizable molecular mechanics study. J Phys Chem B 114:4884
91. Miller Jenkins LM, Hara T, Durell SR, Hayashi R, Inman JK, Piquemal JP, Gresh N, Appella E (2007) Specificity of acyl transfer from 2-mercaptobenzamide thioesters to the HIV-1 nucleocapsid protein. J Am Chem Soc 129:11067
92. Plattner N, Meuwly M (2008) The role of higher CO-multipole moments in understanding the dynamics of photodissociated carbonmonoxide in myoglobin. Biophys J 94:2505
93. Plattner N, Bandi T, Doll J, Freeman DL, Meuwly M (2008) MD simulations using distributed multipole electrostatics: structural and spectroscopic properties of CO- and methane-containing clathrates. Mol Phys 106:1675
94. Devereux M, Plattner N, Meuwly M (2009) Application of multipolar charge models and molecular dynamics simulations to study stark shifts in inhomogeneous electric fields. J Phys Chem A 113:13199

http://www.springer.com/978-3-642-25257-0

Computational Organometallic Chemistry
Wiest, O.; Wu, Y. (Eds.)
2012, VIII, 256 p., Hardcover
ISBN: 978-3-642-25257-0